J Solution Chem (2011) 40: 680–702
DOI 10.1007/s10953-011-9670-x

Solubility Measurements of Crystalline NiO in Aqueous Solution as a Function of Temperature and pH

Donald A. Palmer · Pascale Bénézeth · Caibin Xiao · David J. Wesolowski · Lawrence M. Anovitz

Received: 24 March 2010 / Accepted: 17 September 2010 / Published online: 17 March 2011

Abstract Results of solubility experiments involving crystalline nickel oxide (bunsenite) in aqueous solutions are reported as functions of temperature (0 to 350 °C) and pH at pressures slightly exceeding (with one exception) saturation vapor pressure. These experiments were carried out in either flow-through reactors or a hydrogen-electrode concentration cell for mildly acidic to near neutral pH solutions. The results were treated successfully with a thermodynamic model incorporating only the unhydrolyzed aqueous nickel species (viz., Ni^{2+}) and the neutrally charged hydrolyzed species (viz., $Ni(OH)_2^0$). The thermodynamic quantities obtained at 25 °C and infinite dilution are, with 2σ uncertainties: $\log_{10} K_{s0}^{o} = (12.40 \pm 0.29)$, $\Delta_r G_m^o = -(70.8 \pm 1.7)$ kJ·mol^{-1}; $\Delta_r H_m^o = -(105.6 \pm 1.3)$ kJ·mol^{-1}; $\Delta_r S_m^o = -(116.6 \pm 3.2)$ J·K^{-1}·mol^{-1}; $\Delta_r C_{p,m}^o = (0 \pm 13)$ J·K^{-1}·mol^{-1}; and $\log_{10} K_{s2}^{o} = -(8.76 \pm 0.15)$; $\Delta_r G_m^o = (50.0 \pm 1.7)$ kJ·mol^{-1}; $\Delta_r H_m^o = (17.7 \pm 1.7)$ kJ·mol^{-1}; $\Delta_r S_m^o = -(108 \pm 7)$ J·K^{-1}·mol^{-1}; $\Delta_r C_{p,m}^o = -(108 \pm 3)$ J·K^{-1}·mol^{-1}. These results are internally consistent, but the latter set differs from those gleaned from previous studies recorded in the literature. The corresponding thermodynamic quantities for the formation of Ni^{2+} and $Ni(OH)_2^0$ are also estimated. Moreover, the $Ni(OH)_3^-$ anion was never observed, even in relatively strong basic solutions ($m_{OH^-} = 0.1$ mol·kg^{-1}), contrary to the conclusions drawn from all but one previous study.

Keywords Nickel oxide · Bunsenite · Ni(II) · Solubility · Thermodynamics · Hydrolysis · Aqueous solutions · Temperature · pH

D.A. Palmer (✉) · D.J. Wesolowski · L.M. Anovitz
Chemical Sciences Division, Oak Ridge National Laboratory, P.O. Box 2008, Oak Ridge, TN 37831-6110, USA
e-mail: Solution_Chemistry@comcast.net

P. Bénézeth
Geosciences Environnemental Toulouse (GET), UMR-5563 CNRS/IRD/Université de Toulouse, 14 Avenue Edouard Belin, 31400 Toulouse, France

C. Xiao
Barclay Water Management, Inc., 150 Coolidge Ave., Watertown, MA 02472-2815, USA

1 Introduction

Thermodynamic data for nickel aqueous species are required to understand and model mass transport, deposition and speciation in electric power plant water-steam cycles, especially those in pressurized water reactors, PWRs, where Ni-based alloys play a vital role in their construction. Pourbaix diagrams establish that nickel oxide is stable at PWR operating conditions [1, 2] to just below the hydrogen line, indicating that the potential for stress corrosion cracking, SCC, exists immediately below this field. These diagrams also highlight the importance of defining the vertical pH boundaries, outside of which ionic nickel species (claimed to be predominantly Ni^{2+} and $Ni(OH)_3^-$) are dominant and intragranular SCC becomes an active corrosion mechanism [1, 3].

A combined EXAFS, near-IR and molecular dynamics study [4] of 0.2 mol·kg^{-1} $NiBr_2$ solutions including some with additional 0.8 mol·kg^{-1} NaBr from ambient temperatures to 525 °C concluded that the six-coordinate $Ni(H_2O)_6^{2+}$ structure persists through 325 °C. The transition to a (distorted) tetrahedral four-coordinate structure becomes apparent at 325 °C, enhanced no doubt by the formation of bromide complexes. Therefore, over the temperature range of the current investigation, the octahedral hexaaquonickel(II) ion may be assumed to exist, but the structure of the corresponding hydrolyzed species is a subject for conjecture, although the configuration of the Ni(II) metal center is apparently more resistant to change with temperature and ligand concentration than either those of Co(II) or Zn(II) [4].

In aqueous solution, Ni^{2+} undergoes hydrolysis with increasing pH to form $Ni_m(OH)_n^{2m-n}$ species postulated according to the following equilibria [5]:

$$NiO(cr) + 2H^+ \leftrightharpoons Ni^{2+} + H_2O(l) \tag{1}$$

$$NiO(cr) + H^+ \leftrightharpoons Ni(OH)^+ \tag{2}$$

$$NiO(cr) + H_2O(l) \leftrightharpoons Ni(OH)_2^0 \tag{3}$$

$$NiO(cr) + 2H_2O(l) \leftrightharpoons Ni(OH)_3^- + H^+ \tag{4}$$

$$NiO(cr) + 3H_2O(l) \leftrightharpoons Ni(OH)_4^{2-} + 2H^+ \tag{5}$$

$$NiO(cr) + 1.5H^+ \leftrightharpoons 0.5Ni_2(OH)^{3+} + 0.5H_2O(l) \tag{6}$$

$$NiO(cr) + H^+ \leftrightharpoons 0.25Ni_4(OH)_4^{4+} \tag{7}$$

The speciation dependence on pH can also be expressed in terms of the overall hydrolysis equilibria as follows:

$$Ni^{2+} + H_2O(l) \leftrightharpoons NiOH^+ + H^+ \tag{8}$$

$$Ni^{2+} + 2H_2O(l) \leftrightharpoons Ni(OH)_2^0 + 2H^+ \tag{9}$$

$$Ni^{2+} + 3H_2O(l) \leftrightharpoons Ni(OH)_3^- + 3H^+ \tag{10}$$

$$Ni^{2+} + 4H_2O(l) \leftrightharpoons Ni(OH)_4^{2-} + 4H^+ \tag{11}$$

The hydrolysis constants (at infinite dilution) corresponding to the four last equilibria are respectively defined as K_{11}°, K_{12}°, K_{13}° and K_{14}° in this paper.

There have been four studies of the solubility of NiO (Bunsenite) to high temperatures ($\leq$ 320 °C) carried out over the last three decades [1, 6–8]. The earliest results of Macdonald [1] are very discrepant from those of the later studies. Tremaine and LeBlanc [6] stated that

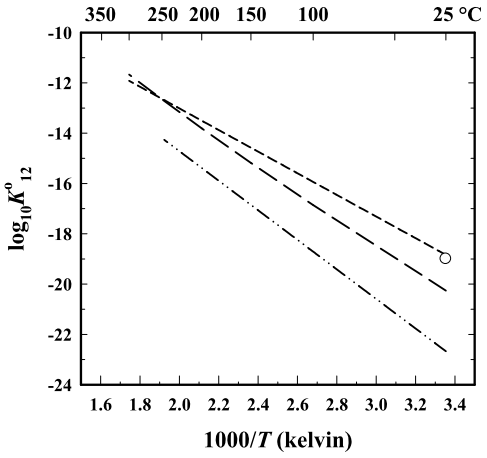

(a)

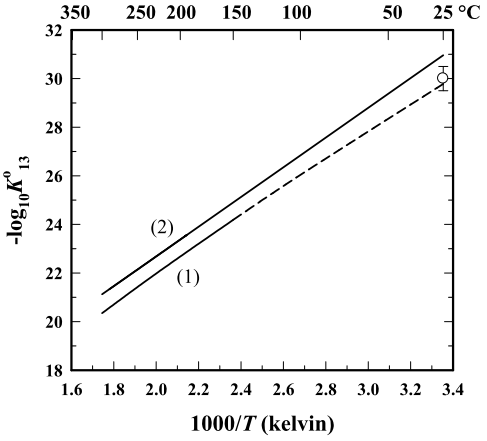

(b)

Fig. 1 (**a**) Logarithm of the second hydrolysis constant of nickel(II) (Eq. 9) versus reciprocal temperature (kelvin) where the data were taken from the studies of: *long-dashed line*, Tremaine and Leblanc [6]; *short-dashed line*, Ziemniak et al. [7]; *dash-dot-dotted line*, Ziemniak et al. [8]; and ○, is the value predicted by Baes and Mesmer [10]. (**b**) Logarithm of the third hydrolysis constant of nickel(II) (Eq. 10) versus reciprocal temperature (kelvin) where *the lines* were taken from the studies of (1) Tremaine and Leblanc [6], and (2) Ziemniak et al. [7], respectively, and the circular symbol represents the value predicted by Baes and Mesmer [10]

the fit of their $\log_{10} K^{\circ}_{s0}$ (Eq. 1) versus temperature data below 200 °C was insensitive to the choice of the $\log_{10} K^{\circ}_{11}$ value (Eq. 8). Ziemniak et al. [7] ignored the presence of $NiOH^+$ in their original data treatment, although it was revised to $-(9.44 \pm 0.11)$ at 25 °C in their later study [8].

The temperature dependence of $\log_{10} K^{\circ}_{12}$ (Eq. 9) was derived by Ziemniak et al. [7] from their solubility data in phosphate-buffered and NaOH solutions, constrained by assuming a constant enthalpy of reaction of $-99.6\ \mathrm{kJ \cdot mol^{-1}}$ [9]. In their more recent study [8], ammonia buffers and NaOH were employed and significantly lower $\log_{10} K^{\circ}_{12}$ values were reported. Both values from the two studies of Ziemniak [7, 8], as well as the $\log_{10} K^{\circ}_{12}$ values extracted from the solubility measurements of Tremaine and Leblanc [6] and the value reported by Baes and Mesmer [10] are shown in Fig. 1a as a function of reciprocal temperature (kelvin).

The lines in Fig. 1b, which represents $\log_{10} K^{\circ}_{13}$ (Eq. 10) as a function of reciprocal temperature, were taken from experiments by Tremaine and LeBlanc [6] from 150 to 300 °C and those of Ziemniak et al. [7] from 17 to 287 °C, whereby $Ni(OH)_2(cr)$ was assumed to be the solubility-limiting phase below 195 °C. Note that the $Ni(OH)_3^-$ species was not detected

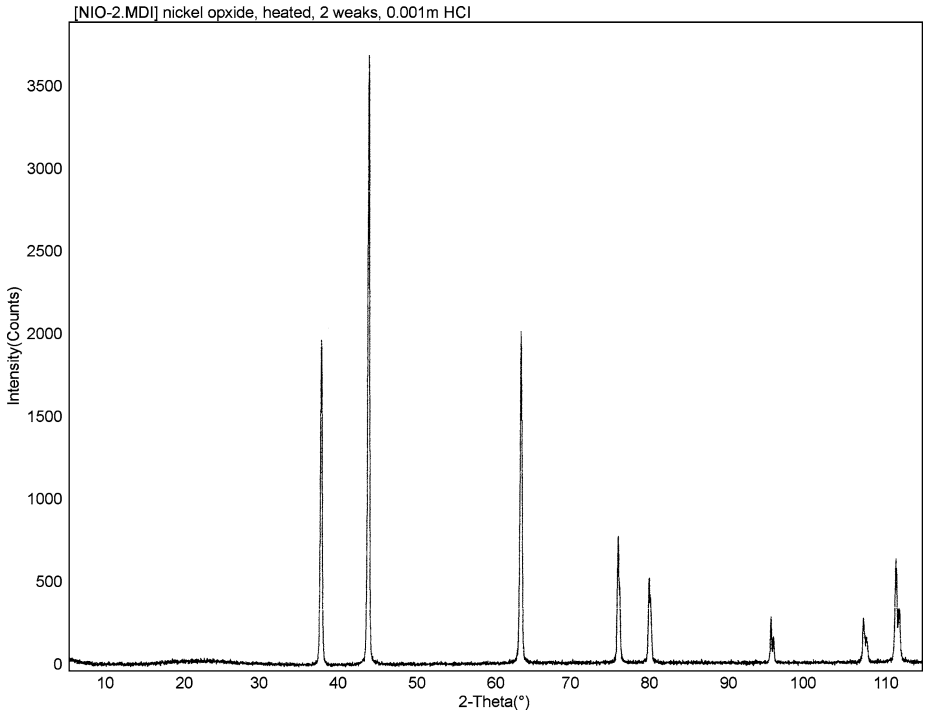

Fig. 2 XRD pattern of NiO crystals (Alfa Aesar Chemical Co.) after heating overnight twice in an air oven to 1000 °C

in the 2004 study by Ziemniak et al. [8]. The $Ni(OH)_4^{2-}$ species was not identified in any of the high-temperature studies carried out to date.

2 Materials and Methods

2.1 Treatment and Characterization of the NiO Solid Phase

Well-crystallized nickel oxide was obtained from Alfa Aesar Chemical Co. (Puratronic® grade, 99.998% (metal basis), lot 22356). In some experiments this material was used as received, but in most cases it was first heated twice overnight in an air oven to 1000 °C to increase the average size and crystallinity of the particles. The XRD pattern and SEM image of this recrystallized NiO are presented in Figs. 2 and 3, respectively. Its surface area as determined by BET (nitrogen) analysis was $(0.26 \pm 0.02)\ cm^2 \cdot g^{-1}$.

2.2 Hydrogen Electrode Concentration Cell (HECC)

The general design and function of the HECC as applied to solubility measurements have been described previously [11] for measurements of the kinetics of dissolution and precipitation near equilibrium [12], and most recently for measurements of the solubility of β-$Ni(OH)_2$(cr) [13]. The use of this cell obviates the need to control pH either by addition of excess acid or base, in which case the pH must be determined by a mass-balance calculation which also requires knowledge of the nickel species in solution (see, Eqs. 8–11), or

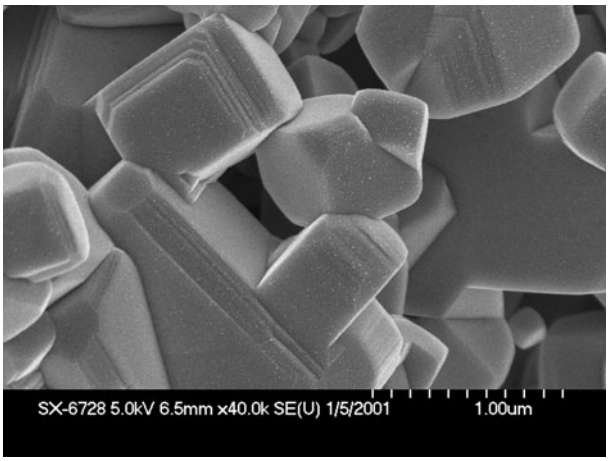

Fig. 3 SEM image of NiO crystals (Alfa Aesar Chemical Co.) after heating overnight twice in an air oven to 1000 °C

through the use of pH buffering agents which might interact with the nickel species in solution to form nickel complexes which enhance the solubility of NiO. Indeed, for this study at low temperatures especially, the former approach cannot be applied to acidic solutions as the solubility is too high, i.e., virtually all the free acid is consumed by reaction 1. However, the HECC was only applicable at low to near-neutral pH, because reduction of the dissolved nickel by the prevailing hydrogen atmosphere became evident at pH values where hydrolysis was significant.

The initial configuration of the cell in a typical NiO solubility experiment involved acidic reference and test solutions (separated by the liquid junction, ‖) as follows:

$$\underset{}{\mathrm{H_2, Pt \mid F_3CSO_3H, F_3CSO_3Na \,\|\, F_3CSO_3H, F_3CSO_3Na, NiO(cr) \mid Pt, H_2}}$$
$$\underset{m_1}{\qquad} \quad \underset{m_2}{\qquad} \quad \underset{m_3}{\qquad} \quad \underset{m_4}{\qquad}$$

The hydrogen ion molality in the test compartment, $m_{\mathrm{H^+}}$, was determined relative to the known molality in the reference compartment, $m_{\mathrm{H^+ref.}}$, from the Nernst equation:

$$\mathrm{pH}_m \equiv -\log_{10} m_{\mathrm{H^+}} = -\log_{10} m_{\mathrm{H^+ref.}} + (E + E_{\mathrm{LJ}})F/(2.3026RT) \tag{12}$$

where T is the temperature expressed in kelvin, E is the measured cell potential, E_{LJ} is the estimated liquid-junction potential calculated from the complete Henderson equation as presented by Baes and Mesmer [10], and F, R and T represent the Faraday constant, universal gas constant and temperature in kelvin, respectively. The largest E_{LJ} values were recorded for the 0.03 mol·kg^{-1} ionic strength titrations (i.e., $|E_{\mathrm{LJ}}| = 4.8$ mV when the test solution was near neutral pH_m, leading to an uncertainty in pH_m of ca. 0.01 [10]).

The inner Teflon cup contained the reference solution of known stoichiometric hydrogen ion molality, whereas the outer cup held the test solution containing a suspension of NiO(cr) (typically ca. 1 g of solid in ca. 65 mL of solution) at the same constant ionic strength employing sodium trifluoromethanesulfonate (F_3CSO_3Na, a non-complexing 1:1 electrolyte). In general, $m_2 = m_4$ at the start of the experiment and the ratio $m_1 : m_2$ (or $m_3 : m_4$) was < 0.1 in order to minimize both liquid-junction contributions to the measured potential and activity coefficient differences between the two solutions. An Ar/H_2 gas mixture was used instead of pure hydrogen to fix the prevailing hydrogen fugacity in order to minimize reduction of the solid phase to metallic nickel. After the initial purging process, which was

repeated eight times to 30 MPa, the hydrogen/argon pressure was regulated to approximately 1 MPa at room temperature.

The temperature was controlled to $\leq \pm 0.1$ °C and was cycled in different directions from different starting values to gauge whether true equilibrium conditions were achieved. Cycling of temperature is equivalent to approaching the equilibrium solubility from under- and over-saturation. Most of the HECC experiments were begun at 100 °C rather than at 25 °C to accelerate the approach to equilibrium, but those begun at lower temperatures gave the same results within the combined experimental error, again indicating that true thermodynamic equilibrium had been established. For measurements made below 25 °C the cell was transferred from the silicon oil bath to a bath containing an ice/water mixture.

Aliquots of the test solution were withdrawn through a porous platinum frit gold-welded to the bottom of a platinum dip tube to prohibit particles from entering the tube that could serve as seeds promoting precipitation during the sampling process. Samples were collected at a titanium valve fitted with a 0.2 μm fluoro-polymer filter into preweighed polypropylene syringes containing a known mass of high purity 0.2% HNO_3 (JT Baker Ultrex Reagent) for subsequent chemical analysis of the nickel content. Generally, a solution sample was collected daily with longer periods being required before the first sample was taken. The self-buffering effect due to the dissolution of NiO(cr) resulted in rather constant Ni concentrations in most of these experiments whereas the pH_m values changed dramatically thereby providing a sensitive indicator of the attainment of equilibrium. Therefore, liquid samples were only taken when the pH_m reading reached a constant value for several hours. The surprising speed with which equilibrium was attained with the HECC especially at low temperatures is attributed to the efficient stirring effect that kept the solid particles suspended exposing all faces to the solution.

2.3 High Temperature Flow Through Cell

This apparatus, which was first described by Bénézeth et al. [14], was used for solubility measurements from 200 to 350 °C. It is important to note that downstream from the outlet closure of the cylindrical reactor, a short section of platinum/rhodium tubing was inserted into the sampling line to serve as a mixing chamber, which allowed a 0.6% nitric acid solution to be pumped into the saturated nickel solution outlet stream at the experimental temperature and pressure, thereby ensuring that nickel hydroxide/oxide did not deposit on the walls of the sampling line. The temperature and pressure stabilities were $< \pm 0.2$ °C and $< \pm 0.3$ MPa, respectively. Samples were generally taken at feed-solution flow rates of 0.03 to 0.3 $mL \cdot min^{-1}$ while the HNO_3 injection rate was ranged from 0.01 to 0.1 $mL \cdot min^{-1}$, respectively.

Dilute trifluoromethanesulfonic acid, ammonia and sodium hydroxide feed solutions were used to control pH. Ammonia becomes a weak ligand for transition metal ions at these high temperatures such that its complexation effect on the prevailing nickel(II) concentration could be ignored [15, 16]. For example, a 2 $mol \cdot kg^{-1}$ NH_3 solution might be expected to produce a ratio $m_{Ni(NH_3)^{2+}}/m_{Ni^{2+}}$ of 0.96 at 25 °C and 0.05 at 200 °C [17]. The higher-order complexes are certainly negligible at high temperatures although the strengths of the mixed aminohydroxo complexes are unknown.

For those experiments, in which mixtures of ammonia and trifluoromethanesulfonic acid was used to buffer the pH_m, an iterative Fortran code was used that took into account the acid-association constant of ammonia:

$$NH_3(aq) + H^+ \leftrightharpoons NH_4^+ \tag{13}$$

taken from the results reported by Hitch and Mesmer [17], namely:

$$\log_{10} Q_{NH_3} = -3.222 + 3048.5/T + 1.1264 \times 10^{-2} T - 1.18917 \times 10^{-5} T^2 \quad (14)$$

where T is the temperature expressed in kelvin.

The isocoulombic nature of this equilibrium allows the assumption that $\log_{10} Q_{NH_3} = \log_{10} K^{o}_{NH_3}$.

2.4 Low Temperature Flow Through Cell

This apparatus [13], which was utilized for five series of solubility measurements at 25 °C and three at 50 °C, consists of three PEEK chromatography columns (25 cm long × 7.5 mm in diameter) connected in series. The columns were submerged in a water bath maintained within ±0.1 °C. The outlet stream was collected into a weighed polypropylene syringe into which a weighed amount of 0.2% ultra pure nitric acid had been added. The syringe and PEEK line leading to it were immersed in the bath as a precaution to prevent deposition before the sample reached the acidified solution in the syringe. An HPLC pump, which exposed the feed solution to only Teflon and sapphire, maintained, in most of the experiments, a constant flow rate of 0.02 mL·min^{-1}, but higher rates up to 0.2 mL·min^{-1} were also used occasionally at 50 °C. Consequently, the approximate residence time for the feed solution in the NiO(cr) bed was ten hours. One series of samples was collected in which boric acid–borate was used as a pH buffer. The main intent of these experiments was to gather data at high pH_m to determine the second NiO solubility constant (Eq. 2), which could not be ascertained from the HECC experiments.

For the single series in which boric acid was used to buffer the pH_m of the solution, the following expression was used [18]:

$$\log_{10} Q_{B(OH)_3} = 3645.18/T + 11.6402 \log_{10} T + (16.4914 - 0.023917T) \log_{10} \rho_w - 36.2605 - 0.11902 I_m - 36.3613 I_m FI/T - 0.72132 I_m^2 \log_{10} \rho_w \quad (15)$$

where: T is the temperature in kelvin, $FI = (1.0 - (1.0 + 2.0 I_m^{0.5}) e^{(-2.0 I_m^{0.5})})/(2.0 I_m)$ and ρ_w is the density of water (g·cm^{-3}) [19].

The appropriate dissociation constant of water, Q_w, was calculated at temperature, T, from Marshall and Franck [20], and the Meissner-based activity coefficients [21] were calculated to determine Q_w at ionic strength I_m. No corrections were required to take into account the dissolution of NiO(cr), because these concentrations were too low to affect the pH_m calculation.

2.5 Sample Handling and Analytical Methods

Samples were collected directly into either polyethylene bottles or polypropylene syringes, which had been presoaked in 0.2% nitric acid for at least 24 hours then rinsed ten times with water immediately prior to use, or presoaked polypropylene syringes containing 0.2% nitric acid (prepared from 70% JT Baker Ultrex Reagent acid). Stock solutions of NaOH, F_3CSO_3H, F_3CSO_3Na, NH_3 and $B(OH)_3$ were prepared from ultra-pure reagents: 50% (by weight) NaOH solution (Mallinckrodt AR grade); concentrated F_3CSO_3H (Alfa Aesar) purified by vacuum distillation; solid F_3CSO_3Na prepared and recrystallized as described in Palmer and Hyde [22] and solid $B(OH)_3$(US Borax). These solutions were prepared with de-aerated Nanopure water and kept under either a helium or argon overpressure.

Nickel analyses were performed by various techniques depending on the nickel concentration in the sample: atomic absorption utilizing a graphite furnace (Perkin Elmer 4110ZL) or flame (Perkin Elmer 3110) spectrophotometer; an ICP (Thermo Jarrell Ash IRIS) or ICP-MS (Finnigan MAT ELEMENT) with two double-focusing sector fields (SF)-ICP-MSearch.

3 Results and Discussion

The experimental results obtained from 0 to 300 °C are summarized in Tables 1, 2 and 3 for solubility data obtained from the HECC experiments, high-temperature flow-cell experiments and low-temperature flow-cell experiments, respectively.

The measured solubility quotients at finite ionic strengths for the equilibria 1 through 5 can be expressed as:

$$Q_{sn} = \frac{m_{\mathrm{Ni(OH)}_n^{2-n}}}{m_{\mathrm{H}^+}^{2-n}} \tag{16}$$

where $m_{\mathrm{Ni(OH)}_n^{2-n}}$ is the molality of the $\mathrm{Ni(OH)}_n^{2-n}$ species and m_{H^+} is the measured or calculated hydrogen ion molality (pH_m is defined as $-\log_{10} m_{\mathrm{H}^+}$). These quotients can then be expressed as solubility constants at infinite dilution:

$$K^{\mathrm{o}}_{sn} = Q_{sn}\gamma_{\mathrm{Ni(OH)}_n^{2-n}} a_{\mathrm{w}}^{1-n}/\gamma_{\mathrm{H}^+}^{2-n} \tag{17}$$

In Eq. 17, $\gamma_{\mathrm{Ni(OH)}_n^{2-n}}$ represents the activity coefficient of the $\mathrm{Ni(OH)}_n^{2-n}$ species for $n = 0$–4, γ_{H^+} symbolizes the activity coefficient of the hydrogen ion and a_{w} is the water activity.

In view of the generally low ionic strengths employed in this work, $\gamma_{\mathrm{Ni(OH)}_2^0}$ for the neutrally charged species is assumed to be unity. The activity coefficients for the other Ni species were derived from the Meissner equation [21] with the implicit assumption that for an ion of charge, $z : \gamma_{|z|} = \gamma_{\pm(\mathrm{NaCl})}^{z^2}$, where $\gamma_{\pm(\mathrm{NaCl})}$ is the molal single-ion activity coefficient of NaCl. The advantage of this approach is that accurate $\gamma_{\pm(\mathrm{NaCl})}$ values are available from Archer [19] over the entire temperature range accessed in this investigation. The corresponding water activities were also taken from Archer [19]. Table 4 lists activity coefficients calculated from the simple Debye-Hückel equation, as favored previously [6, 7], and the Meissner equation (i.e., those for NaCl [19]) and experimental values for NaOH [24] which was the dominant electrolyte in the high pH_m flow-cell experiments. For the HECC experiments, the Ni^{2+} and H^+ were minor components of the electrolyte mixture dominated by $\mathrm{F_3CSO_3Na}$.

An excellent review of nickel chemistry [5] established that neither the bi- nor tetranuclear Ni species defined in Eqs. 6 and 7 were significant at the nickel concentrations employed in the present study so that (from Eqs. 1–5) the total or measured molality of nickel(II) in solution is given by:

$$\begin{aligned} m_{\mathrm{Ni}} &= m_{\mathrm{Ni}^{2+}} + m_{\mathrm{Ni(OH)}^+} + m_{\mathrm{Ni(OH)}_2^0} + m_{\mathrm{Ni(OH)}_3^-} + m_{\mathrm{Ni(OH)}_4^{2-}} \\ &= Q_{\mathrm{s}0} m_{\mathrm{H}^+}^2 + Q_{\mathrm{s}1} m_{\mathrm{H}^+} + Q_{\mathrm{s}2} + Q_{\mathrm{s}3}/m_{\mathrm{H}^+} + Q_{\mathrm{s}4}/m_{\mathrm{H}^+}^2 \end{aligned} \tag{18}$$

Figure 4 depicts the dependence of the logarithm of the nickel molality on pH_m corrected to infinite dilution at 25 °C. The symbols represent the individual data points from the HECC and flow-cell techniques with the solid curve being derived from fits of the combined results of this study (Eqs. 20 and 21 which are discussed below). It can readily be seen that despite

Table 1 Summary of the solubility data for nickel oxide from the HECC experiments (the experimental uncertainty in $\log_{10} K^{o}_{s0}$ is given as 2σ)

Run Nr.	t/ °C	p/ MPa	a_w	I_m	pH$_m$	$\gamma_{\pm(NaCl)}$	$\log_{10} m_{Ni}$	$\log_{10} K^{o}_{s0}$
18-9	0.3	5.9	0.9989	0.0307	8.718	0.852	−3.200	14.10 ± 0.05
18-10	0.3	6.1	0.9989	0.0307	8.727	0.852	−3.189	14.13 ± 0.05
17-8	4.0	6.3	0.9989	0.0316	8.552	0.851	−2.790	14.17 ± 0.05
17-9	4.1	6.6	0.9989	0.0316	8.565	0.851	−2.790	14.20 ± 0.05
18-7	4.5	5.5	0.9989	0.0307	8.575	0.853	−3.202	13.81 ± 0.05
18-8	4.4	5.6	0.9989	0.0307	8.582	0.853	−3.202	13.82 ± 0.05
17-6	24.9	5.7	0.9989	0.0317	7.707	0.847	−2.786	12.48 ± 0.05
17-7	24.9	6.2	0.9989	0.0317	7.749	0.847	−2.792	12.56 ± 0.05
18-5	24.7	5.5	0.9989	0.0307	7.909	0.849	−3.199	12.48 ± 0.05
18-6	24.7	5.5	0.9989	0.0307	7.911	0.849	−3.200	12.48 ± 0.05
18-3	49.7	4.4	0.9989	0.0307	7.042	0.843	−3.205	10.73 ± 0.05
18-4	49.7	5.0	0.9989	0.0307	7.042	0.843	−3.206	10.73 ± 0.05
17-4	50.0	5.9	0.9989	0.0317	6.946	0.842	−2.787	10.96 ± 0.05
17-5	50.0	6.0	0.9989	0.0317	6.922	0.841	−2.788	10.91 ± 0.05
18-1	99.9	2.9	0.9989	0.0307	6.075	0.826	−3.218	8.77 ± 0.05
18-2	99.9	3.1	0.9989	0.0307	6.076	0.826	−3.219	8.77 ± 0.05
17-1	100.0	4.2	0.9989	0.0316	5.834	0.824	−2.800	8.70 ± 0.05
17-2	99.8	4.5	0.9989	0.0316	5.822	0.824	−2.798	8.68 ± 0.05
17-3	99.9	5.2	0.9989	0.0316	5.833	0.824	−2.801	8.70 ± 0.05
3-5	152.4	2.6	0.9990	0.0252	6.076	0.815	−4.393	7.58 ± 0.05
3-6	152.5	2.5	0.9990	0.0252	6.067	0.814	−4.416	7.54 ± 0.05
3-7	152.4	2.6	0.9990	0.0252	6.060	0.814	−4.411	7.53 ± 0.05
3-8	152.4	2.6	0.9990	0.0252	6.050	0.815	−4.427	7.50 ± 0.05
3-1	152.4	2.5	0.9990	0.0296	5.321	0.803	−3.321	7.13 ± 0.05
3-2	152.5	2.5	0.9990	0.0296	5.327	0.803	−3.321	7.14 ± 0.05
3-3	152.4	2.5	0.9990	0.0296	5.331	0.803	−3.321	7.15 ± 0.05
3-4	152.4	2.5	0.9990	0.0296	5.330	0.803	−3.321	7.15 ± 0.05
4-2	149.6	2.1	0.9990	0.0305	5.260	0.803	−3.294	7.04 ± 0.05
4-3	149.6	2.2	0.9990	0.0305	5.106	0.803	−3.310	6.71 ± 0.05
4-4	149.7	2.2	0.9990	0.0305	4.990	0.803	−3.320	6.47 ± 0.05
4-1	149.7	2.0	0.9990	0.0306	5.269	0.803	−3.292	7.06 ± 0.05
5-1	150.1	2.5	0.9990	0.0307	5.231	0.802	−3.248	7.02 ± 0.05
4-5	149.7	2.9	0.9990	0.0327	4.612	0.798	−2.819	6.21 ± 0.05
4-6	149.7	3.0	0.9990	0.0330	4.584	0.797	−2.782	6.19 ± 0.05
13-3	149.8	2.9	0.9967	0.1006	5.095	0.712	−3.264	6.63 ± 0.06
13-4	149.8	3.0	0.9967	0.1006	5.203	0.712	−3.275	6.84 ± 0.06
13-5	149.9	3.2	0.9967	0.1006	5.220	0.712	−3.281	6.86 ± 0.06
16-1	149.7	3.4	0.9967	0.1010	5.046	0.705	−3.184	6.60 ± 0.06
7-1	149.7	3.1	0.9966	0.1028	4.702	0.711	−2.947	6.16 ± 0.06
7-2	149.7	3.0	0.9966	0.1028	4.797	0.711	−2.959	6.34 ± 0.06
7-3	149.9	3.2	0.9966	0.1028	4.777	0.711	−2.957	6.30 ± 0.06
7-4	149.7	3.2	0.9966	0.1028	4.767	0.711	−2.956	6.28 ± 0.06
12-6	149.8	3.5	0.9903	0.3018	4.751	0.628	−2.785	6.31 ± 0.07
10-1	149.8	2.6	0.9903	0.3019	4.642	0.628	−2.760	6.12 ± 0.07
11-4	149.9	3.1	0.9903	0.3019	4.889	0.628	−2.765	6.60 ± 0.07

Table 1 (*Continued*)

Run Nr.	t/ °C	p/ MPa	a_w	I_m	pH_m	$\gamma_{\pm(NaCl)}$	$\log_{10} m_{Ni}$	$\log_{10} K^{o}_{s0}$
11-5	149.9	3.2	0.9903	0.3019	4.891	0.628	−2.767	6.61 ± 0.07
12-7	149.8	3.7	0.9903	0.3019	4.756	0.628	−2.780	6.32 ± 0.07
12-5	149.8	4.6	0.9903	0.3020	4.748	0.629	−2.768	6.32 ± 0.07
3-9	203.3	4.0	0.9992	0.0254	5.578	0.783	−4.602	6.34 ± 0.05
3-10	203.3	4.1	0.9992	0.0254	5.559	0.783	−4.598	6.31 ± 0.05
3-11	203.4	4.2	0.9992	0.0254	5.539	0.783	−4.583	6.28 ± 0.05
3-12	203.4	4.2	0.9992	0.0254	4.817	0.783	−3.389	6.03 ± 0.05
3-13	203.3	4.2	0.9992	0.0254	4.811	0.783	−3.383	6.03 ± 0.05
3-14	203.4	4.2	0.9992	0.0254	4.805	0.783	−3.451	5.95 ± 0.05
2-1	203.3	3.6	0.9990	0.0297	4.607	0.771	−3.379	5.61 ± 0.05
2-2	203.3	3.6	0.9990	0.0297	4.526	0.771	−3.370	5.46 ± 0.05
2-3	203.3	3.6	0.9990	0.0297	4.435	0.771	−3.371	5.27 ± 0.05
2-4	203.3	3.7	0.9990	0.0297	4.546	0.771	−3.747	5.12 ± 0.05
5-3	199.9	3.7	0.9990	0.0306	4.462	0.771	−3.283	5.42 ± 0.05
5-2	200.0	3.9	0.9990	0.0307	4.501	0.771	−3.276	5.50 ± 0.05
5-4	199.9	4.1	0.9990	0.0307	4.434	0.771	−3.265	5.38 ± 0.05
5-5	199.8	4.1	0.9989	0.0328	4.177	0.766	−2.807	5.32 ± 0.05
5-6	199.7	3.9	0.9989	0.0329	4.171	0.765	−2.796	5.31 ± 0.05
13-1	199.9	4.1	0.9968	0.1007	4.603	0.667	−3.283	5.57 ± 0.06
13-6	199.9	4.4	0.9968	0.1007	4.786	0.667	−3.282	5.94 ± 0.06
13-7	199.9	4.7	0.9968	0.1007	4.771	0.667	−3.283	5.91 ± 0.06
13-8	199.9	4.9	0.9968	0.1007	4.789	0.667	−3.295	5.93 ± 0.06
13-2	199.9	4.2	0.9968	0.1008	4.650	0.667	−3.269	5.68 ± 0.06
14-1	199.5	6.0	0.9967	0.1021	4.338	0.667	−3.114	5.21 ± 0.06
14-2	199.5	5.9	0.9967	0.1024	4.311	0.667	−3.041	5.23 ± 0.06
7-6	199.8	4.7	0.9967	0.1029	4.220	0.665	−2.968	5.12 ± 0.06
7-5	199.8	4.7	0.9967	0.1030	4.227	0.665	−2.961	5.14 ± 0.06
8-1	199.8	3.7	0.9906	0.3027	4.067	0.568	−2.752	4.89 ± 0.07
8-2	199.8	3.5	0.9906	0.3026	4.125	0.568	−2.770	4.99 ± 0.07
8-3	199.8	3.7	0.9906	0.3026	4.113	0.568	−2.767	4.96 ± 0.07
8-4	199.8	3.7	0.9906	0.3025	4.143	0.568	−2.782	5.01 ± 0.07
11-1	199.8	4.3	0.9906	0.3020	4.359	0.569	−2.817	5.41 ± 0.07
11-2	199.8	4.4	0.9906	0.3022	4.392	0.569	−2.793	5.50 ± 0.07
11-3	199.8	4.5	0.9906	0.3023	4.389	0.569	−2.782	5.50 ± 0.07
11-6	199.8	5.0	0.9906	0.3022	4.322	0.569	−2.767	5.38 ± 0.07
12-1	199.8	4.9	0.9906	0.3020	4.353	0.569	−2.831	5.38 ± 0.07
12-2	199.8	4.9	0.9906	0.3024	4.263	0.569	−2.779	5.25 ± 0.07
12-3	199.8	5.0	0.9906	0.3025	4.251	0.569	−2.763	5.25 ± 0.07
12-4	199.8	5.0	0.9906	0.3024	4.251	0.569	−2.777	5.23 ± 0.07
3-15	254.3	7.2	0.9992	0.0254	4.311	0.740	−3.494	4.87 ± 0.06
3-16	254.3	7.3	0.9992	0.0254	4.292	0.740	−3.454	4.87 ± 0.06
3-17	254.2	7.4	0.9992	0.0254	4.271	0.740	−3.441	4.84 ± 0.06
5-7	249.6	6.8	0.9989	0.0330	3.659	0.721	−2.810	4.22 ± 0.06
5-8	249.5	6.6	0.9989	0.0329	3.642	0.721	−2.816	4.18 ± 0.06
5-9	249.5	6.5	0.9989	0.0330	3.545	0.721	−2.815	3.99 ± 0.06
5-10	249.5	7.6	0.9989	0.0328	3.588	0.722	−2.831	4.06 ± 0.06

Table 1 (*Continued*)

Run Nr.	t/ °C	p/ MPa	a_w	I_m	pH_m	$\gamma_{\pm(NaCl)}$	$\log_{10} m_{Ni}$	$\log_{10} K^o_{s0}$
6-1	249.6	5.6	0.9990	0.0306	4.143	0.727	−3.334	4.67 ± 0.06
6-2	249.6	5.6	0.9990	0.0305	4.072	0.727	−3.396	4.47 ± 0.06
7-7	249.9	7.2	0.9968	0.1038	3.842	0.603	−2.875	4.37 ± 0.07
7-8	249.9	7.1	0.9968	0.1038	3.839	0.603	−2.870	4.37 ± 0.07
8-5	249.8	6.3	0.9910	0.3033	3.789	0.490	−2.766	4.19 ± 0.08
12-8	249.9	8.0	0.9910	0.3026	3.909	0.491	−2.822	4.37 ± 0.08
12-9	250.0	7.9	0.9911	0.3027	3.905	0.491	−2.812	4.38 ± 0.08
13-9	250.0	7.6	0.9969	0.1008	4.222	0.606	−3.321	4.69 ± 0.07
14-3	249.6	8.9	0.9968	0.1024	3.848	0.606	−3.048	4.21 ± 0.07
14-4	249.6	8.9	0.9968	0.1022	3.891	0.606	−3.108	4.24 ± 0.07
16-8	250.1	7.9	0.9969	0.1008	3.923	0.606	−3.380	4.03 ± 0.07
16-9	250.1	8.4	0.9969	0.1009	3.923	0.606	−3.361	4.05 ± 0.07
16-10	250.1	8.7	0.9969	0.1006	3.902	0.607	−3.334	4.04 ± 0.07
8-6	289.9	9.9	0.9916	0.3032	3.541	0.408	−2.810	3.49 ± 0.09
3-18	300.1	12.4	0.9992	0.0262	3.817	0.681	−3.540	3.76 ± 0.06
3-19	300.1	12.4	0.9992	0.0263	4.025	0.680	−3.542	4.17 ± 0.06
3-20	300.1	12.4	0.9992	0.0263	3.998	0.680	−3.530	4.13 ± 0.06
7-9	302.5	12.5	0.9970	0.1031	3.497	0.511	−3.007	3.40 ± 0.08
13-10	297.1	12.3	0.9970	0.1007	3.995	0.526	−3.315	4.12 ± 0.08
14-5	299.6	14.1	0.9970	0.1017	3.481	0.522	−3.141	3.26 ± 0.08
16-11	289.9	12.3	0.9970	0.1017	3.657	0.540	−3.351	3.43 ± 0.08

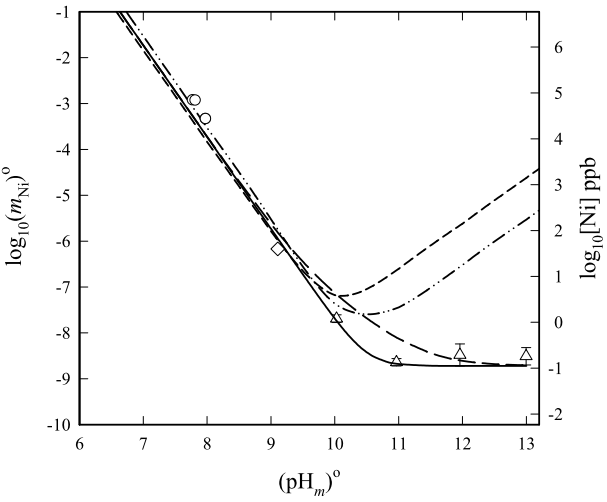

Fig. 4 Solubility profile for NiO(cr) at 25 °C and infinite dilution where the symbols Δ and ◊ represent results from the low-temperature flow-cell experiments in NaOH and $B(OH)_3$–NaOH buffered solutions, respectively, and ○ represents results obtained with the HECC. *The solid line* was generated from Eqs. 20 and 21, whereas *the long-dashed curve* included the proposed $\log_{10} K^o_{11}$ value of $-(9.54 \pm 0.14)$ [5]. *The short-dashed* and *dot-dot-dashed curves* were determined according to Tremaine and Leblanc [6], and the model of Shock et al. [25], respectively

the good agreement at low pH_m between the current results and those of Tremaine and Leblanc [6], at $pH_m > 9.5$ the results diverge with far lower solubilities evidenced from the current study that can be traced to the absence of the $Ni(OH)_3^-$ species and especially the $Ni(OH)_4^{2-}$ species, leaving the $Ni(OH)_2^0$ species to dominate completely at high pH_m.

Table 2 Summary of results for the solubility of NiO(cr) from the high-temperature flow-cell experiments with flow rates of 0.1 and 0.3 mL·min^{-1} for the F_3SO_3H, NH_3 and NaOH buffer feed solutions, respectively (No. sam. refers to the number of samples analyzed)[a]

t/ °C	No. sam.	p / MPa	$m_{F_3CSO_3H} \times 10^{-3}$	$m_{NH_3} \times 10^{-3}$	$m_{NaOH} \times 10^{-3}$	$I_m \times 10^{-3}$	a_w	pH_m	$\gamma_{\pm}$(NaCl)	$\log_{10} m_{Ni}$	$\log_{10} K^o_{s0}$	$\log_{10} K^o_{s2}$
200.0	4	13.1	0	0	12.5	12.5	0.9996	9.168	0.838	−7.88 ± 0.24		−7.9 ± 0.2
200.0	13	13.5	0	0	1.16	1.16	1.0000	8.236	0.943	−8.15 ± 0.17		−8.2 ± 0.2
200.0	9	13.5	0	0	0.148	0.148	1.0000	7.373	0.979	−8.15 ± 0.05		−8.2 ± 0.1
200.0	6	15.0	0	1.05	0	0.617	1.0000	6.991	0.957	−8.15 ± 0.06		−8.2 ± 0.1
200.0	10	15.0	1.97	5.80	0	1.98	0.9999	6.073	0.927	−5.72 ± 0.05	6.36 ± 0.09	
200.0	12	15.0	1.02	5.97	0	1.04	1.0000	6.462	0.945	−6.24 ± 0.07	6.63 ± 0.10	
200.0	9	15.0	0.553	1.68	0	0.561	1.0000	6.088	0.959	−5.85 ± 0.05	6.29 ± 0.09	
200.0	9	14.0	0	0	104.4	104.4	0.9967	9.887	0.668	−8.34 ± 0.09		−8.3 ± 0.1
250.0	9	12.0	0	0	104.4	104.4	0.9968	9.705	0.606	−8.07 ± 0.10		−8.1 ± 0.1
250.0	9	12.0	0	0	29.7	29.7	0.9990	9.324	0.733	−8.58 ± 0.40		−8.6 ± 0.4
250.0	10	12.0	0	0	1.12	1.12	1.0000	8.108	0.932	−8.71 ± 0.21		−8.7 ± 0.2
250.0	6	12.0	0	0	0.145	0.145	1.0000	7.259	0.974	−8.59 ± 0.78		−8.6 ± 0.8
250.0	8	12.0	3.73	5.04	0	3.78	0.9999	4.769	0.882	−4.27 ± 0.05	5.16 ± 0.09	
250.0	13	12.0	1.18	3.49	0	1.19	1.0000	5.460	0.930	−5.92 ± 0.07	4.94 ± 0.10	
250.0	9	12.0	0.303	3.50	0	0.315	1.0000	6.174	0.963	−7.30 ± 0.18	5.02 ± 0.19	
250.0	11	12.0	0	0	0.150	0.150	1.0000	7.273	0.974	−8.64 ± 0.08		−8.6 ± 0.1
300.0	11	14.0	0	0	0.150	0.150	1.0000	7.423	0.967	−8.23 ± 0.32		−8.2 ± 0.3
300.0	8	14.0	0	0	1.12	1.12	1.0000	8.250	0.914	−8.44 ± 0.15		−8.4 ± 0.2
300.0	10	14.0	0	0	10.01	10.0	0.9997	9.060	0.778	−8.34 ± 0.17		−8.3 ± 0.2
300.0	13	11.6	0	1.04	0	0.014	1.0000	6.471	0.990	−8.35 ± 0.19		−8.4 ± 0.2
300.0	8	11.6	0.504	1.99	0	0.505	1.0000	5.059	0.940	−7.50 ± 0.27	2.56 ± 0.28	
300.0	8	11.6	1.24	2.06	0	1.24	1.0000	4.448	0.909	−5.22 ± 0.02	3.59 ± 0.07	
300.0	12	11.6	0.209	2.02	0	0.210	1.0000	5.520	0.961	−7.68 ± 0.41	3.33 ± 0.48	
300.0	16	11.6	0.529	1.99	0	0.529	1.0000	5.033	0.939	−6.67 ± 0.10	3.34 ± 0.12	

Table 2 (*Continued*)

t/ °C	No. sam.	p / MPa	$m_{F_3CSO_3H} \times 10^{-3}$	$m_{NH_3} \times 10^{-3}$	$m_{NaOH} \times 10^{-3}$	$I_m \times 10^{-3}$	a_w	pH$_m$	$\gamma_{\pm(NaCl)}$	$\log_{10} m_{Ni}$	$\log_{10} K^o_{s0}$	$\log_{10} K^o_{s2}$
300.0	9	11.6	0	0	98.2	98.2	0.9971	9.776	0.521	−8.29 ± 0.35		−8.3 ± 0.4
350.0	20	17.8	0	0	1.50	1.50	0.9999	9.217	0.855	−8.47 ± 0.75		−8.5 ± 0.8
350.0	15	17.8	0	0	0.107	0.107	1.0000	8.170	0.958	−9.15 ± 0.26		−9.2 ± 0.3
350.0	16	17.8	0	1.99	0	0.004	1.0000	6.720	0.992	−8.79 ± 0.18		−8.8 ± 0.2
350.0	21	17.8	0.148	2.04	0	0.148	1.0000	5.080	0.951	−8.65 ± 0.28		−8.7 ± 0.3
350.0	21	17.8	1.02	2.03	0	1.02	1.0000	4.033	0.878	−5.66 ± 0.03	2.29±0.08	
350.0	16	17.4	1.84	0	0	2.44	0.9999	3.190	0.819	−3.23 ± 0.01	2.98±0.05	
350.0	19	18.1	0.209	1.99	0	0.209	1.0000	4.909	0.942	−7.56 ± 0.25	2.21±0.26	
350.0	17	18.1	0.501	0	0	0.592	1.0000	3.497	0.906	−4.04 ± 0.02	2.87±0.06	
350.0	13	18.1	0	0	12.2	12.2	0.9996	9.882	0.661	−8.88 ± 0.39		−8.9 ± 0.4
350.0	20	18.1	0	0	12.6	12.6	0.9996	9.888	0.657	−8.96 ± 0.29		−9.0 ± 0.3
350.0	17	26.6	0	0	12.6	12.6	0.9996	9.490	0.691	−8.82 ± 0.62		−8.8 ± 0.6
350.0	9	26.6	1.31	0	0	1.65	0.9999	3.207	0.867	−3.47 ± 0.02	2.82±0.06	
350.0	6	16.0[b]	0	0	0	0	1.0000	–	1.000	−9.53 ± 0.19		

[a]The $\log_{10} m_{Ni}$ values represent the average from multiple samples collected at each condition and the associated uncertainties are simply the averages of these analyses

[b]Deionized water was used as the feed solution for which the saturation vapor pressure at this condition is 16.5 MPa

Table 3 Summary of results for the solubility of NiO(cr) at 0.1 MPa from the low-temperature flow-cell experiments at a flow rate of 0.02 mL·min^{-1} (No. sam. refers to the number of samples analyzed)[a,b]

t/ °C	No. sam.	$m_{B(OH)_3} \times 10^{-3}$	$m_{NaOH} \times 10^{-3}$	$I_m \times 10^{-3}$	a_w	pH_m	$\gamma_{\pm(NaCl)}$	$\log_{10} m_{Ni}$	$\log_{10} K^o_{s0}$	$\log_{10} K^o_{s2}$
24.9	14	0	1.00	1.00	1.0000	10.981	0.965	-8.64 ± 0.08		-8.6 ± 0.1
25.0	9	0	0.108	0.108	1.0000	10.022	0.988	-7.68 ± 0.08	12.35 ± 0.12	
25.0	14	0	9.21	9.21	0.9997	11.917	0.906	-8.48 ± 0.24		-8.5 ± 0.2
25.0	12	0	100.1	100.1	0.9966	12.886	0.777	-8.51 ± 0.19		-8.5 ± 0.2
49.9	12	0	100.1	100.1	0.9967	12.164	0.770	-8.46 ± 0.32		-8.5 ± 0.3
50.0	12	0	12.5	12.5	0.9996	11.319	0.888	-9.05 ± 0.38		-9.0 ± 0.4
50.0	12	0	1.01	1.01	1.0000	10.264	0.963	-8.84 ± 0.12		-8.8 ± 0.1
25.0	10	2.28	0.964	0.967	1.0000	9.107	0.966	-6.14 ± 0.03	12.04 ± 0.09	

[a]The $\log_{10} m_{Ni}$ values represent the average from multiple samples collected at each condition and the associated uncertainties are simply the averages of these analyses

[b]The experimental uncertainty (2σ) in $\log_{10} K^o_{s0}$ was determined to be 0.17 with the most significant contribution coming from the pH_m measurement

Table 4 Calculated activity coefficients computed from different sources

t/ °C	I_m/mol·kg^{-1}	γ_{H^+} Meissner[a]	γ_{H^+} DH[b]	$\gamma_{(Na^+,OH^-)}$ exper.[c]	$\gamma_{Ni^{2+}}$ Meissner
0	0.03	0.854	0.857		0.53
25	0.03	0.850	0.851		0.52
50	0.03	0.844	0.844		0.51
100	0.03	0.827	0.826		0.47
150	0.03	0.803	0.803		0.42
150	0.1	0.712	0.710	0.706	0.26
150	0.3	0.628	0.619		0.16
200	0.03	0.772	0.773		0.36
200	0.1	0.667	0.670	0.652	0.20
200	0.3	0.568	0.570		0.10
250	0.03	0.727	0.731		0.28
250	0.1	0.604	0.614	0.578	0.13
250	0.3	0.488	0.504		0.057
300	0.03	0.660	0.663		0.19
300	0.1	0.513	0.527		0.069
300	300/0.3	0.380	0.407		0.021
350	0.013	0.641	0.656		0.17

[a]These values result from the Meissner approximation [21] (see text)

[b]DH represents the simple Debye-Hückel term as used by Tremaine and Leblanc [6] whose flow-cell experiments were conducted at $I_m \leq 0.0373$ mol·kg^{-1}, viz. $\log_{10}\gamma = -z^2 A\{I_m^{0.5}/(1 + 1.5I_m^{0.5})\}$ where A was calculated according to Silvester and Pitzer [23]

[c]Taken from tabulated values for single electrolyte NaOH solutions by Holmes and Mesmer [24] representing those cases where the maximum NaOH concentration was used

Although these solubility data are not sufficiently accurate to rule out the existence of the $Ni(OH)^+$ cation over a narrow pH_m range, they do not support the proposed $\log_{10} K^{\circ}_{11}$ (Eq. 8) by the NEA [5].

Figure 5 displays the corresponding results obtained at 300 °C where it is even more obvious that the $Ni(OH)_2^0$ species dominates from near neutral to $pH_m = 10.06$ (ca. 0.1 mol·kg^{-1} NaOH). Although the solubility minima reported in two of the earlier high-temperature solubility studies [6, 7] are close to those predicted from the current results, again no increase in solubility at high pH_m is apparent ruling out the formation of the $Ni(OH)_3^-$ (and $Ni(OH)_4^{2-}$) species under the prevailing experimental conditions. A similar observation was made in the second investigation by Ziemniak and coworkers [8]. Again the stability of the intermediate hydrolyzed species $Ni(OH)^+$ cannot be accessed from the current results. Note that the results predicted by Shock et al. [25] are only shown because of their importance in the commonly used geochemical model SUPCRT.

No definitive explanation can be offered at this time as to why the higher-order trihydroxo anion was not observed at any temperature to $m_{OH^-} = 0.1$ mol·kg^{-1}, whereas in the case of the analogous ZnO system, solubility constants of all three hydrolyzed species were derived unambiguously [14, 26], noting however that Ni^{2+} tends to hydrolyze at a significantly higher pH than does the Zn^{2+} and resists more strongly a configuration change to a tetrahedral geometry [4]. This finding is significant, particularly for the nuclear power in-

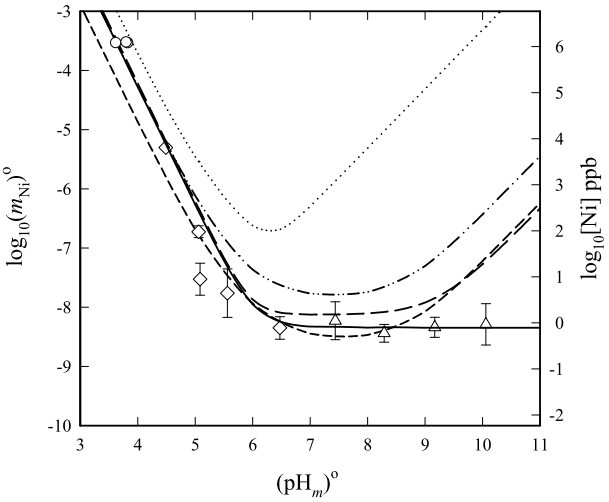

Fig. 5 Solubility profile for NiO(cr) at 300 °C and infinite dilution where the symbols Δ and ◊ represent results from the high-temperature flow-cell experiments in NaOH and NH_3–F_3CSO_3H buffered solutions, respectively, and ○ represents results obtained with the HECC. *The solid curve* was generated from Eqs. 20 and 21, whereas the remaining curves were taken from: *short-dashed*, Tremaine and Leblanc [6]; *long-dashed*, Ziemniak et al. [7]; *dot-dot-dashed*, the model of Shock et al. [25]; *dotted*, Macdonald and Cragnolino [1], respectively

dustry, in that according to these new results a wide range of pH operating conditions is available under which nickel alloy dissolution would be constant and minimal.

From the above discussion it is apparent that the reactions that only need to be considered in the treatment of the current solubility results, listed in Tables 1, 2 and 3, are defined by Eqs. 1 and 3.

3.1 First Solubility Constant

The first solubility constant with the appropriate activity coefficients and water activity is derived from:

$$K_{s0}^{o} = m_{Ni^{2+}}\gamma_{Ni^{2+}}a_w^2/m_{H^+}^2\gamma_{H^+}^2 = Q_{s0}\gamma_{Ni^{2+}}a_w^2/\gamma_{H^+}^2 \tag{19}$$

In accordance with Eq. 19, the $\log_{10} m_{Ni}$, $\gamma_{|z|}$, a_w and pH_m values in Tables 1, 2 and 3 were used to calculate $\log_{10} K_{s0}^{o}$ as reported in the last column of these tables. The simplest equation that provided the best fit of these data using a weighted linear least-squares regression is shown in Eq. 20

$$\log_{10} K_{s0}^{o} = -(6.093 \pm 0.167) + (5513.46 \pm 69.73)/T \tag{20}$$

The plot of $\log_{10} K_{s0}^{o}$ versus reciprocal temperature (T/K) is given in Fig. 6 showing all the experimental results from this study. The data in Fig. 6 clearly indicate a linear relationship within the experimental scatter over the temperature range, 0 to 350 °C, and the values obtained by the three techniques for the various solid phases at different ionic strengths and media are concordant. This agreement, coupled with the number of experiments carried out with the HECC using two different starting acidities and different starting temperatures, which were varied and sometimes cycled in different directions give a high degree of confidence that equilibrium was always established. In view of the low temperatures investigated where NiO(cr) is metastable with respect to $Ni(OH)_2$(s), it was deemed especially important to establish this fact. This is also supported with the use of Fig. 7, showing an XRD pattern of the washed solid material reclaimed from an HECC experiment (series 18, see Table 1)

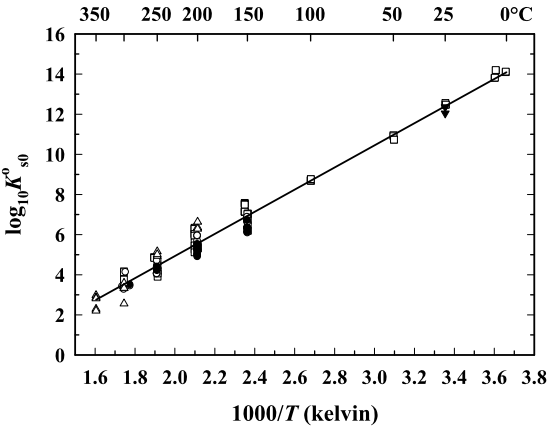

Fig. 6 The dependence of $\log_{10} K^{o}_{s0}$ on the reciprocal temperature (kelvin) where *the solid line* results from the weighted linear two-term fit (Eq. 20) of the data in Tables 1, 2 and 3 and the symbols: □, ○ and ● represent 0.03, 0.1 and 0.3 mol·kg^{-1} ionic strength, respectively, taken from the results in Table 1 (HECC); ▼ and △ represent results obtained with the high- and low-temperature flow reactors listed in Tables 2 and 3, respectively

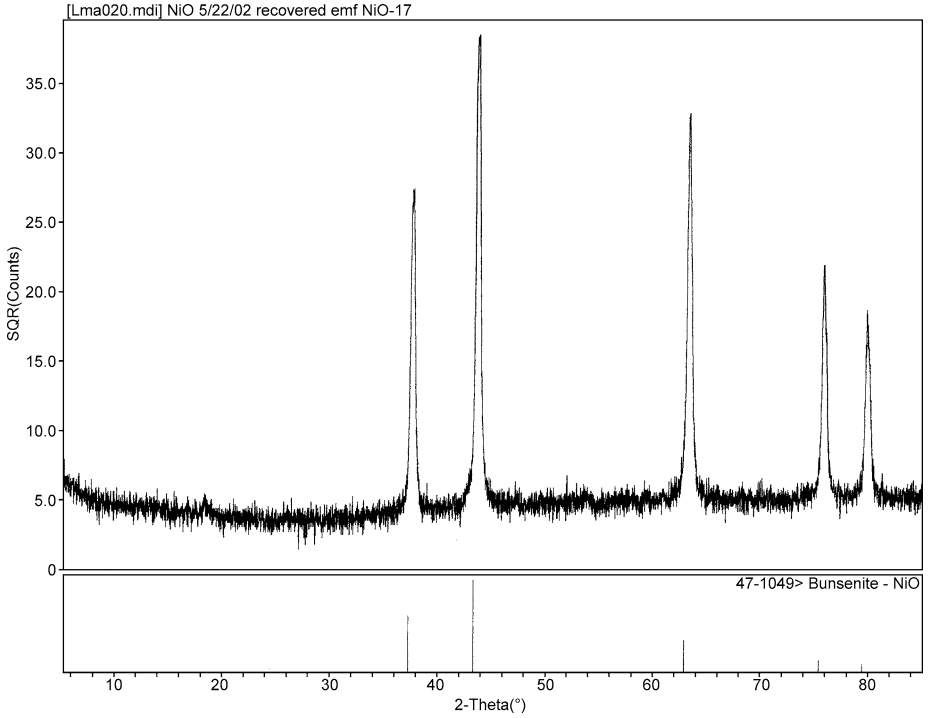

Fig. 7 XRD of solid recovered (after washing with de-ionized water) from a HECC experiment (series 18-samples 1/10) showing that the bulk of the material corresponds to crystalline NiO, but with indication of a small peak at a 2θ of 19° that could be attributed to $Ni(OH)_2$(cr) which has major peaks at 19.17, 33.05, 38.48, 51.94, 59.02, and 62.66°, where all but the first are partially screened by the major NiO peaks. Note that there is a slight offset of the peaks relative to the NiO standard that is due to a misalignment of the instrument

terminated at 0.3 °C, which is well below the thermal stability range of the NiO starting material. The major peaks corresponded to crystalline NiO with possibly a small occurrence of $Ni(OH)_2$(cr) (a small peak at a 2θ of 19°). Furthermore, the measured solubility at this low

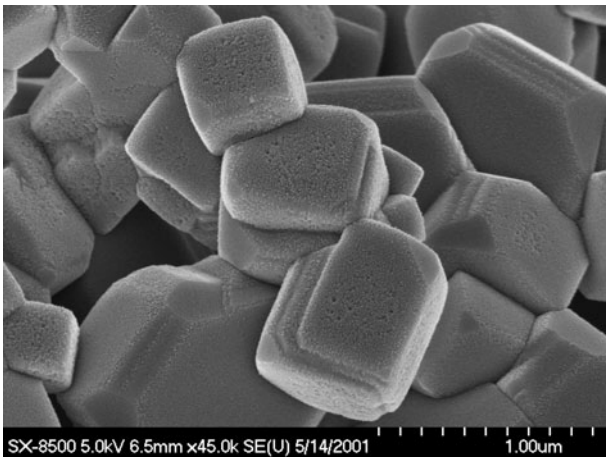

Fig. 8 SEM image of NiO crystals recovered from HECC after completion of experiment 3 (samples 1–20). Etching of crystal faces due to dissolution in acidic solution is clearly visible

temperature was substantially higher than that of $Ni(OH)_2$(cr) obtained from independent HECC experiments [13], indicating quite logically that the NiO higher-energy phase still controlled the equilibrium solubility. This is further evidence that the kinetics of transformation of the oxide and hydroxide phases are very sluggish at low temperatures [27].

No physical degradation of the solid particles was evident from the SEM and BET surface area analyses of the NiO(cr) particles measured before and after the HECC experiments but some nickel metal was discovered (verified by XRD analysis) in experiments conducted at $\geq 150\,^{\circ}C$, in the test cup after the experiment was terminated. However, the nickel oxide recovered from the exit end of the high-temperature flow reactor (after the entire sampling series was completed and after first pumping pure water through the reactor at the final temperature of 350 °C for several days, then purging with helium during the quenching process) was found to have a surface area of $(0.74 \pm 0.04)\ cm^2 \cdot g^{-1}$. The XRD pattern of this material showed only NiO(cr). This unusual increase in surface area could be possibly attributable to the de-aggregation of the NiO crystal clusters over time. On the other hand, after washing the solid material recovered from the HECC experiments with water and drying under vacuum, the SEM image in Fig. 8 showed no appreciable de-aggregation, but did show clear evidence of dissolution etch pits on the crystal surfaces. The surface area of this solid did not change measurably from that of the starting material. However, it must be remembered that: (1) this solid was exposed only to acidic solutions where the solubility is appreciable; (2) this solid was suspended in the acidic solution whereas the solid recovered from the end of the flow reactor was most likely only exposed to solutions already saturated with nickel(II); (3) the duration of the HECC experiments was much shorter (one or two weeks versus many months) where the temperature rarely reached 300 °C, and then for less than 24 hours.

Equation 20 gives a $2\sigma \log_{10} K^{\circ}_{s0}$ value at 25 °C of (12.40 ± 0.29), which compares favorably with (12.48 ± 0.15) recommended by the NEA [5] based on more accurate EMF and heat-capacity data. The other thermodynamic quantities obtained from this equation, and its first and second derivatives with respect to T at 25 °C are: $\Delta_r G^{\circ}_m = -(70.8 \pm 1.7)\ kJ \cdot mol^{-1}$; $\Delta_r H^{\circ}_m = -(105.6 \pm 1.3)\ kJ \cdot mol^{-1}$; $\Delta_r S^{\circ}_m = -(116.6 \pm 3.2)\ J \cdot K^{-1} \cdot mol^{-1}$; $\Delta_r C^{\circ}_{p,m} = (0 \pm 13)\ J \cdot K^{-1} \cdot mol^{-1}$, cf. $\Delta_r G^{\circ}_m = -(71.2 \pm 0.9)\ kJ \cdot mol^{-1}$; $\Delta_r H^{\circ}_m = -(101.1 \pm 1.0)\ kJ \cdot mol^{-1}$; $\Delta_r S^{\circ}_m = -(100.3 \pm 1.5)\ J \cdot K^{-1} \cdot mol^{-1}$; $\Delta_r C^{\circ}_{p,m} = -(15 \pm 8)\ J \cdot K^{-1} \cdot mol^{-1}$ from [5] based on the thermodynamic quantities given in Table 5. Attempts to either impose a constraint on the fit by adopting either recommended

Table 5 Summary of the thermodynamic quantities at 25.0 °C

Species	$\Delta_f G_m^o$ kJ·mol^{-1}	$\Delta_f H_m^o$ kJ·mol^{-1}	S_m^o J·K^{-1}·mol^{-1}	$C_{p,m}^o$ J·K^{-1}·mol^{-1}	Reference
NiO(cr)	-211.66 ± 0.42	-239.70 ± 0.40	38.40 ± 0.40	44.40 ± 0.10[a]	[5]
NiO(cr)	-211.7	-239.7[a]	37.99[a]	44.31	[9]
H_2O(l)	-237.14 ± 0.04	-285.83 ± 0.04	69.95 ± 0.03	75.35 ± 0.08	[5]
H_2O(l)	-237.13	-285.83	69.91	75.2	[9]
Ni^{2+}	-45.77 ± 0.77	-55.01 ± 0.88	-131.9 ± 1.4	-46.1 ± 7.5	[5]
Ni^{2+}	-45.6	-54.0	-128.9	–	[9]
Ni^{2+}	-45.5 ± 3.4	-54.1 ± 2.5	-129 ± 5	–	[28]
Ni^{2+}	-45.52	-54.04	-128.9	–	[29]
Ni^{2+}	-45.3 ± 1.8	-59.5 ± 1.4	-148.2 ± 3.2	-31 ± 13	This work[b]
$Ni(OH)_2^0$	-398.8 ± 1.8	-507.8 ± 1.7	0.4 ± 7.0	11.8 ± 3.0	This work[b]

[a]Taken from Hemingway [30]

[b]Using the relevant thermodynamic quantities recommended by Gamsjäger et al. [5]

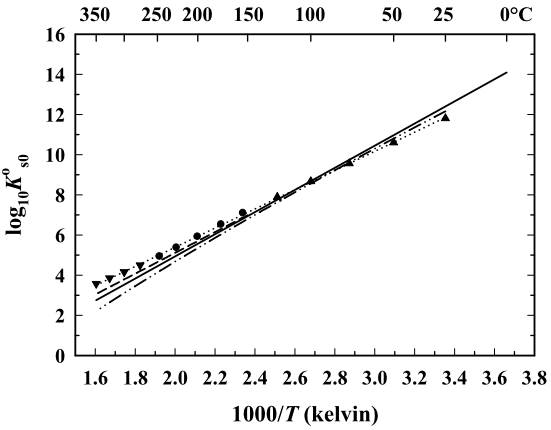

Fig. 9 The dependence of $\log_{10} K_{s0}^o$ on the reciprocal temperature (kelvin) where *the solid line* stems from Eq. 20, whereas *the short-dashed* and *dash-dot-dotted curves* were taken from the studies of Tremaine and Leblanc [6], and Ziemniak et al. [7], respectively. The symbols ▲, ● and ▼ result from regressions reported by Ziemniak et al. [8] for the solid phases, $Ni(OH)_2$(cr), *rhombohedral* NiO(cr) and *cubic* NiO(cr), respectively, with *the dotted line* representing a simple linear regression the combined data for all three solid phases

entropy or heat-capacity values for NiO(cr) [5] at 25 °C or by introducing an additional temperature-dependent variable into Eq. 20 produced fits where at least one other thermodynamic quantity was at greater variance from the recommended values [5]. Therefore, Eq. 20 was retained as the most conservative representation of the results obtained in this research.

Note that in the fit of their NiO(cr) solubility data (150–300 °C) shown in Fig. 9, Tremaine and Leblanc [6] restrained their model by adopting $\Delta_r G_m^o$ and $\Delta_r S_m^o$ values at 25 °C of -69.400 kJ·mol^{-1} and -100.2 J·K^{-1}·mol^{-1}. Their fit agrees extremely well with Eq. 20 deviating slightly but systematically with increasing temperature. The earlier results of Ziemniak et al. [7] show larger and negative deviations, noting that included in the fit presented in Fig. 9 are their results for β-$Ni(OH)_2$(cr) solubility below 190 °C that we consider to be assigned ambiguously to this phase. This conclusion is supported by the fact that the duration of their experiments was much shorter than those of the current study where no such transformation was observed. Moreover, in the more recent reinvestigation by Ziemniak et al. [8], report the appearance of apparent discontinuities with temperature in the

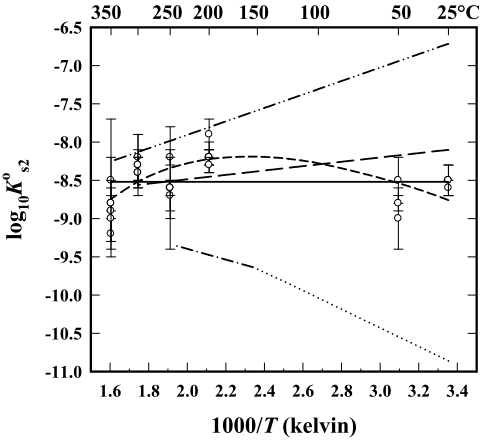

Fig. 10 The dependence of $\log_{10} K^{\circ}_{s2}$ on the reciprocal temperature (kelvin) where *short dashed curve* resulted from the weighted two-term fit (Eq. 21) of the data in Tables 2 and 3, and *the solid line* is the simple average value of $\log_{10} K^{\circ}_{s2}$. *The dash-dot-dotted* and *long-dashed lines* were generated from regressions by Tremaine and Leblanc [6], and Ziemniak et al. [7]. *The dash-dot-dashed* and *dotted lines* were generated from the thermodynamic quantities supplied by Ziemniak et al. [8] for the solid phases NiO(cr) and $Ni(OH)_2$(cr), respectively

solubility constant for NiO(cr) at 149 and 247 °C were assigned to the solid-phase transformation due to dehydration of β-$Ni(OH)_2$(cr) and to a subsequent rhombohedral to a cubic morphology change, respectively. In fact the latter transformation was reported to cause an increased temperature dependence of $\log_{10} K^{\circ}_{s0}$, which is thermodynamically unreasonable as it implies the formation of a less stable cubic structure. As can be seen from these data in Fig. 9, all of their results can be fitted to a single linear function within experimental uncertainty limits, although the deviation at high temperatures from the current result is outside those limits. Thus, the solid-phase transformation of NiO(cr) from rhombohedral to cubic is believed to be too slow at these moderate temperatures (247–315 °C, where moderate refers to solid-state transformations) to affect the solubility data.

From Eq. 20 and the analogous equation for the β-$Ni(OH)_2$(cr) solubility constant, the temperature for the conversion of the latter to NiO(cr) in aqueous solution is calculated to be 89 °C, which is 12 °C higher than that calculated in our previous paper [13], which was based on the $\log_{10} K^{\circ}_{s0}$ data for NiO(cr) of Tremaine and Leblanc [6]. However, despite the uncertainty of the current estimate, it is still substantially lower than those proposed in the literature [6–8] with the caveat that particle size is an important factor in determining the true thermodynamic stability of β-$Ni(OH)_2$(cr) [13] even for particles with $>$ 1 μm cross section, so that transition temperatures $>$ 89 °C could have resulted if larger β-$Ni(OH)_2$(cr) particles had been investigated. Finally, it must be remembered that in the previous high-temperature solubility studies involving NiO(cr) [6–8], β-$Ni(OH)_2$ crystals were believed to have formed in situ during temperature cycling experiments and would therefore have probably been very fine grained.

3.2 Second Solubility Constant

A number of functions of temperature were explored for the $\log_{10} K^{\circ}_{s2}$ data in Tables 2 and 3. Although a linear fit in $1/T$ would be the most conservative representation, apart from declaring a temperature-independent value considering the large uncertainties in these values, Eq. 21 is proposed as providing the best representation of these results (see Fig. 10)

$$\log_{10} K^{\circ}_{s2} = -(1769.2 \pm 40.1)/T - (0.0094755 \pm 0.0002016)T \tag{21}$$

Assuming a temperature-independent $\log_{10} K^{\circ}_{s2}$ value would have led to an average of $-(8.52 \pm 0.31)$ at 25 °C, whereas a weighted fit according to Eq. 21 gave a value

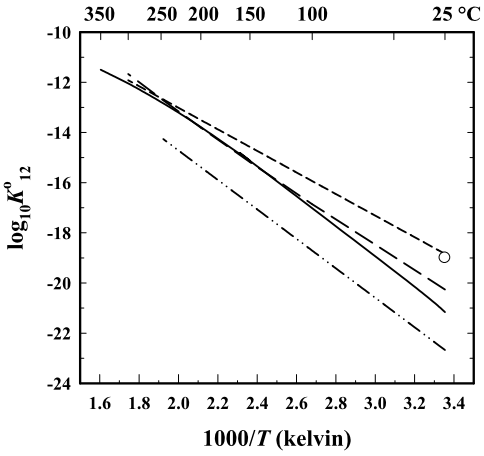

Fig. 11 Logarithm of the second hydrolysis constant of nickel(II) (Eq. 9) versus reciprocal temperature (kelvin) where *the solid line* was generated from Eq. 22 and the *remaining lines* were taken from the studies as designated in Fig. 1a

of $-(8.76 \pm 0.15)$. Inclusion of a constant temperature-independent term produced a very poor fit, whereas substituting a $\ln(T)$ term for the T term gave a marginally poorer fit. Equation 21 yielded the thermodynamic quantities at 25 °C: $\Delta_r G_m^o = (50.0 \pm 1.7)$ kJ·mol^{-1}; $\Delta_r H_m^o = (17.7 \pm 1.7)$ kJ·mol^{-1}; $\Delta_r S_m^o = -(108 \pm 7)$ J·K^{-1}·mol^{-1}; and $\Delta_r C_{p,m}^o = -(108 \pm 3)$ J·K^{-1}·mol^{-1}. The estimated thermodynamic quantities for $Ni(OH)_2^0$ are given in Table 5 based on those recommended by Gamsjäger et al. [5].

Figure 10 illustrates that the results from previous studies [6, 8] tend to converge at higher temperatures range but show large and opposite deviations approaching ambient conditions (noting that the fit by Tremaine and Leblanc [5] of their high temperature was anchored by thermodynamic quantities at 25 °C for the Ni species [31, 32] and those for water [9]). Sluggish kinetics of dissolution coupled with problems such as the presence of fine particulates which are difficult to remove and sample contamination have probably contributed to the scatter in these earlier results.

The last entry in Table 2 corresponds to an experiment in which the pressure at 350 °C was lowered slightly below the saturation vapor pressure of water, viz., 16.53 MPa, resulting in a density drop from the experiment at 26.6 MPa from 0.6314 to 0.1024 g·cm^{-3}. Pressure is the prime variable in determining the stability of solutes in steam giving rise to the lower $\log_{10} K_{s2}^o$ value of $-(9.5 \pm 0.2)$ corresponding to a solubility of 0.017 ppb, which is considerably less than reported for the more soluble ZnO(cr), namely 1 ppb, at this condition [14].

3.3 Second Hydrolysis Constant

By combining Eqs. 20 and 21, an equation for the second hydrolysis constant was calculated as follows:

$$\log_{10} K_{12}^o = (6.09 \pm 0.17) - (7282.7 \pm 80.4)/T - (0.009476 \pm 0.000202)T \qquad (22)$$

The values derived from Eq. 22 are shown and compared with the corresponding literature values in Fig. 11. As can be seen from this figure, the present values are in good agreement with those calculated from the solubility measurements of Tremaine and Leblanc [6] over the temperature range of their measurements.

4 Conclusions

Results of the current investigation are in very reasonable agreement with those of Tremaine and Leblanc [6] for $\log_{10} K^{o}_{s0}$ and extend over a wider temperature range. The $\log_{10} K^{o}_{s0}$ value at 25 °C is also concordant with that obtained from a recent exhaustive review of aqueous nickel chemistry [5]. At higher pH_m the results are not sufficiently precise to allow any determination of the value of $\log_{10} K^{o}_{s1}$, although previous estimates appear to be too high [5–7]. As first mentioned by Ziemniak et al. [8], the $\log_{10} K^{o}_{s3}$ values reported in the literature appear to have been also vastly overestimated with no evidence for the existence of the $Ni(OH)_3^-$ anion being found under any of the experimental conditions investigated here. The experimental uncertainty in the $\log_{10} K^{o}_{s2}$ values reported here is admittedly large but clearly establish the dominance and hence importance to PWR corrosion issues of the $Ni(OH)_2^0$ species over a wide range of near neutral to basic conditions.

A companion study [13] of $Ni(OH)_2$(cr) solubility yielded $\log_{10} K^{o}_{s0}$ as a function of temperature to 200 °C using the same experimental techniques described here. Interestingly, a striking particle size effect was identified that extended to much larger particle sizes than expected adding undoubtedly to the wide disparity of constants reported previously in the literature. The corresponding data for NiO(cr) in acidic to near neutral pH solutions are more consistent suggesting more typical particle-size independent solubility behavior for particles > 1 μm. Note also that from this recent study the dehydration temperature of $Ni(OH)_2$(cr) to NiO(cr) was given as 77 °C (cf. 89 °C determined in the current study), 100 °C or more lower than reported previously [5–8].

Acknowledgements All of the experimental work was carried out in the Chemical Sciences Division of ORNL under sponsorship of the U.S. Department of Energy under the NEPO initiative in collaboration with EPRI, Inc., Palo Alto, California with project managers Paul Frattini and Keith Frazzetti.

References

1. Macdonald, D.D., Cragnolino, G.A.: Corrosion of steam cycle materials. In: Cohen, P. (ed.) The ASME Handbook on Water Technology for Thermal Power Plants (1989). EPRI Project No. RP 1958–1, Chap. 9
2. Beverskog, B., Puigdomenech, I.: Revised Pourbaix diagrams for nickel at 25–300 °C. Corros. Sci. **39**, 969–980 (1997)
3. Kritzer, P., Boukis, N., Dinjus, E.: Factors controlling corrosion in high-temperature aqueous solutions: a contribution to the dissociation and solubility data influencing corrosion processes. J. Supercrit. Fluids **15**, 205–227 (1999)
4. Hoffmann, M.M., Darab, J.G., Palmer, B.J., Fulton, J.L.: A transition in the Ni^{2+} complex structure from six- to four-coordinate upon formation of ion pair species in supercritical water: an X-ray absorption fine structure, near-infrared, and molecular dynamics study. J. Phys. Chem. **103**, 8471–8482 (1999)
5. Gamsjäger, H., Bugajski, J., Gajda, T., Lemire, R.J., Preis, W.: In: Mompean, F., Illemasséne, M., Perrone, J. (eds.) Chemical Thermodynamics of Nickel. Elsevier, Amsterdam (2005), Chap. V
6. Tremaine, P.R., LeBlanc, J.C.: The solubility of nickel oxide and hydrolysis of Ni^{2+} in water to 573 K. J. Chem. Thermodyn. **12**, 521–538 (1980)
7. Ziemniak, S.E., Jones, M.E., Combs, K.E.S.: Solubility and phase behavior of nickel oxide in aqueous sodium phosphate solutions at elevated temperatures. J. Solution Chem. **18**, 1133–1152 (1989)
8. Ziemniak, S.E., Goyette, M.A.: Nickel(II) oxide solubility and phase stability in high temperature aqueous solutions. J. Solution Chem. **33**, 1135–1159 (2004)
9. Wagman, D.D., Evans, W.H., Parker, V.B., Schumm, R.H., Halow, I., Bailey, S.M., Churney, K.L., Nuttall, R.L.: The NBS tables of chemical thermodynamic properties. J. Phys. Chem. Ref. Data **11**, 2–38 (1982) 2–166
10. Baes, C.F., Jr., Mesmer, R.E.: The Hydrolysis of Cations. Wiley, New York (1976)

11. Palmer, D.A., Bénézeth, P., Wesolowski, D.J.: Aqueous high temperature solubility studies. I. The solubility of boehmite at 150 °C as a function of ionic strength and pH as determined by "in situ" measurements. Geochim. Cosmochim. Acta **65**, 2081–2095 (2001)
12. Bénézeth, P., Palmer, D.A., Wesolowski, D.J.: Dissolution/precipitation kinetics of boehmite: application of a pH relaxation technique to study near-equilibrium rates. Geochim. Cosmochim. Acta **72**, 2429–2453 (2008)
13. Palmer, D.A., Gamsjäger, H.: Solubility measurements of crystalline β-$Ni(OH)_2$ in aqueous solution as a function of temperature and pH. J. Coord. Chem. **63**, 2888–2908 (2010)
14. Bénézeth, P., Palmer, D.A., Wesolowski, D.J., Xiao, C.: New measurements of the solubility of zinc oxide from 150 to 350 °C. J. Solution Chem. **31**, 947–973 (2002)
15. Mironov, V.E., Pashkov, G.L., Stupko, T.V.: Thermodynamics of formation reactions and hydrometallurgical application of metal-ammonia complexes in aqueous solutions. Russ. Chem. Rev. **61**, 944–958 (1992)
16. NIST Critically selected stability constants of metal complexes database. Version 6.0 for Windows, NIST Standard Reference Database 46 (2001)
17. Hitch, B.F., Mesmer, R.E.: The ionization of aqueous ammonia to 300 °C in KCl media. J. Solution Chem. **5**, 667–680 (1976)
18. Palmer, D.A., Bénézeth, P., Wesolowski, D.J.: Boric acid hydrolysis: a new look at the available data. PowerPlant Chem. **2**, 261–264 (2000)
19. Archer, D.G.: Thermodynamic properties of the $NaCl + H_2O$ system. II. Thermodynamic properties of NaCl(aq), $NaCl{\cdot}2H_2O$(cr), and phase equilibria. J. Phys. Ref. Data **21**, 793–829 (1992)
20. Marshall, W.L., Franck, E.U.: Ion product of water substance, 0–1000 °C, 1–10,000 bars. New international formulation and its background. J. Phys. Chem. Ref. Data **10**, 295–304 (1981)
21. Lindsay, W.T., Jr.: In: Cohen, P. (ed.) The ASME Handbook on Water Technology for Thermal Power Plants, p. 483. The American Society of Mechanical Engineers, New York (1989), Chap. 7
22. Palmer, D.A., Hyde, K.E.: Ferrous chloride and acetate complexation in aqueous solutions at high temperatures. Geochim. Cosmochim. Acta **57**, 1393–1408 (1993)
23. Sylvester, L.F., Pitzer, K.S.: Thermodynamics of electrolytes. 8. High-temperature properties, including enthalpy and heat capacity, with application to sodium chloride. J. Phys. Chem. **81**, 1822–1828 (1977)
24. Holmes, H.F., Mesmer, R.E.: Isopiestic molalities for aqueous solutions of the alkali metal hydroxides at elevated temperatures. J. Chem. Thermodyn. **30**, 311–326 (1998)
25. Shock, E.L., Sassani, D.C., Willis, M., Sverjensky, D.A.: Inorganic species in geologic fluids: correlations among standard molal thermodynamic properties of aqueous ions and hydroxide complexes. Geochim. Cosmochim. Acta **61**, 907–950 (1997)
26. Bénézeth, P., Palmer, D.A., Wesolowski, D.J.: The solubility of zinc oxide in 0.03 m NaTr as a function of temperature with in situ pH measurement. Geochim. Cosmochim. Acta **63**, 1571–1586 (1999)
27. Swaddle, T.W., Wong, T.C.T.: Hydrothermal reaction kinetics. The decomposition of nickel(II) hydroxide. Can. J. Chem. **56**, 363–369 (1978)
28. Plyasunova, N.V., Zhang, Y., Muhammed, M.: Critical evaluation of thermodynamics of complex formation of metal ions in aqueous solutions. IV. Hydrolysis and hydroxo-complexes of Ni^{2+} at 298.15 K. Hydrometallurgy **48**, 43–63 (1998)
29. Archer, D.G.: Thermodynamic properties of importance to environmental processes and remediation. II. Previous thermodynamic property values for nickel and some of its compounds. J. Phys. Chem. Ref. Data **28**, 1485–1507 (1999)
30. Hemingway, B.S.: Thermodynamic properties for bunsenite, NiO, magnetite, Fe_3O_4, and hematite, Fe_2O_3, with comments on selected oxygen buffer reactions. Geochim. Cosmochim. Acta **75**, 781–790 (1990)
31. Boyle, B.J., King, E.G., Conway, K.C.: Heats of formation of nickel and cobalt oxides (NiO and CoO) of combustion calorimetry. J. Am. Chem. Soc. **76**, 3835–3837 (1954)
32. Kelley, K.K., King, E.G.: Contributions to the data on theoretical metallurgy. XIV. Entropies of the elements and inorganic compounds. U.S. Bur. Mines Bull. No. 592 (1961)